The 2013 World Congress on
Advances in Structural Engineering and Mechanics (ASEM13)
Jeju, Korea, September 8-12, 2013

The elastoplastic Cosserat continuum model and numerical simulation of strain localization

*Hong-xiang Tang[1)] and Zhao-long Hu[2)]

[1), 2)] *School of Civil Engineering, Faculty of Infrastructure Engineering, Dalian University of Technology, Dalian 116024, China*
[1)] *tanghx@dlut.edu.cn*

ABSTRACT

The elastoplastic Cosserat continuum models for both two and three dimensional pressure-dependent materials are presented in this paper. The non-associated Drucker-Prager yield criterion is particularly considered. The size effects of a cantilever beam, the mesh-independent solution of a shear structure, the strain localization failure due to strain softening in excavation and the strain localization failure due to material dilatancy in retaining structure are studied by the developed model with corresponding finite element methods. Numerical results illustrate that the present finite element methods based on the proposed Cosserat continuum models are capable of reflecting the size effects, ensuring mesh-independent solution, preserving the well-posedness of the boundary value problem characterized by the strain localization due to strain softening and material dilatancy and simulating the entire progressive failure process occurring in engineering structures.

1. Introduction

When strain softening constitutive behavior or non-associated yield criterion in certain condition is incorporated into a computational model in the frame of classical plastic continuum, the initial and boundary value problem of the model will become ill-posed, resulting in pathologically mesh-dependent solutions (Troncone 2005, Pande and Pietruszczak 1986, Li et al 2002).

To accurately simulate strain localization phenomena characterized by occurrence and severe development of the deformation localized into narrow bands of intense irreversible strain caused by strain softening or the non-associated plasticity, it is required to introduce some type of regularization mechanism into the classical continuum model to preserve the well-posedness of the localization problem. One of the radical approaches to introduce the regularization mechanism into the model is to utilize

[1)] Professor
[2)] Graduate Student

the Cosserat micro-polar continuum theory, in which high-order continuum structures are introduced. Among the work, which utilize the Cosserat continuum model as the regularization approach to analyze strain localization problems, are contributions of (Muhlhaus et al 1987, Muhlhaus 1989； de Borst et al 1991, de Borst 1991,1993; Tejchman et al 1993, 1996； Steinmann 1994, 1999；lordache and Willam 1998; Manzari 2004; Li and Tang 2005; Khoei et al 2007). (Ehlers et al 1998) presented the theoretical and numerical methods for micropolar elasto-plastic solid materials in the framework of the Theory of Porous Media.

The above-mentioned research on Cosserat continuum is mainly focused on 2D plane strain problems, despite the fact that the actual engineering structures are usually three dimensional. In three dimensional Cosserat continuum, there are six independent degrees-of-freedom at each material point, i.e. three conventional translational degrees of freedom and three rotational degrees of freedom, and eighteen stress components with corresponding strain components including the torsional and bending components, which makes the Cosserat theory more appropriate in predicting the deformation of the structure when it bears a tensional moment or bending moment. Recently, (Rubin 2005; Liu et al. 2007; Azadeh and Curran 2009; Azadeh et al. 2009) contributed to the numerical solution of structures such as shells, cantilevers and plates based on three dimensional Cosserat theories. Application to solid continuum, (Khoei et al 2010) formulated an elasto-plastic pressure-independent J2 flow model within the framework of the Cosserat continuum.

In this paper, we present the elastoplastic Cosserat continuum models for both two and three dimensional pressure-dependent materials. To reveal the capability and performance of the models developed, the size effects of a cantilever beam, the mesh-independent solution of a shear structure, and the strain localization phenomena due to strain softening and material dilatancy are analyzed with corresponding finite element methods. Numerical results illustrate that as compared with the performance of the finite element procedure based on the classical continuum model, the present finite element methods based on the proposed Cosserat continuum models are capable of reflecting the size effects, ensuring mesh-independent solution, preserving the well-posedness of the boundary value problem characterized by the strain localization due to strain softening and material and dilatancy and simulating the entire progressive failure process occurring in engineering structures.

2. The governing equations of elastic Cosserat continuum

2.1 2D Cosserat continuum

Each material point in the two dimensional Cosserat continuum has three degrees-of-freedom, i.e. two translational degrees-of-freedom u_x, u_y and one rotational degree-of-freedom ω_z with the rotation axis orthogonal to the two dimensional plane,

$$\mathbf{u} = [u_x \; u_y \; \omega_z]^{\mathrm{T}} \tag{1}$$

Correspondingly, the strain and stress vectors are defined as

$$\boldsymbol{\varepsilon} = [\varepsilon_{xx}\ \varepsilon_{yy}\ \varepsilon_{zz}\ \varepsilon_{xy}\ \varepsilon_{yx}\ \kappa_{zx} l_c\ \kappa_{zy} l_c]^{\mathrm{T}} \tag{2}$$

$$\boldsymbol{\sigma} = [\sigma_{xx}\ \sigma_{yy}\ \sigma_{zz}\ \sigma_{xy}\ \sigma_{yx}\ m_{zx}/l_c\ m_{zy}/l_c]^{\mathrm{T}} \tag{3}$$

where κ_{zx}, κ_{zy} are introduced as micro-curvatures in Cosserat theory, m_{zx}, m_{zy} are the couple stresses conjugate to the curvatures κ_{zx}, κ_{zy}, l_c is defined as the internal length scale. Fig. 1 gives stress and couple-stress in a two-dimensional Cosserat continuum.

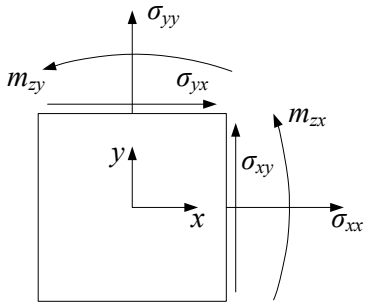

Fig. 1 Stress and couple-stress in a two-dimensional Cosserat continuum

The relation between strain components and displacement components and the equilibrium equations can be written in matrix – vector forms as

$$\boldsymbol{\varepsilon} = \mathbf{L}\mathbf{u} \tag{4}$$

$$\mathbf{L}^{\mathrm{T}}\boldsymbol{\sigma} + \mathbf{f} = \mathbf{0} \tag{5}$$

in which the operator matrix

$$\mathbf{L}^{\mathrm{T}} = \begin{bmatrix} \frac{\partial}{\partial x} & 0 & 0 & 0 & \frac{\partial}{\partial y} & 0 & 0 \\ 0 & \frac{\partial}{\partial y} & 0 & \frac{\partial}{\partial x} & 0 & 0 & 0 \\ 0 & 0 & 0 & -1 & 1 & l_{\mathrm{c}} \frac{\partial}{\partial x} & l_{\mathrm{c}} \frac{\partial}{\partial y} \end{bmatrix} \tag{6}$$

It is assumed that the strain vector $\boldsymbol{\varepsilon}$ is decomposed into both the elastic and the plastic parts, i.e. $\boldsymbol{\varepsilon}_e$ and $\boldsymbol{\varepsilon}_p$, and the elastic strain vector $\boldsymbol{\varepsilon}_e$ is linearly related to the stress vector,

$$\boldsymbol{\sigma} = \mathbf{D}_e \boldsymbol{\varepsilon}_e \tag{7}$$

in which the elastic modulus matrix $\mathbf{D}_e$ for isotropic media can be given in the form

$$\mathbf{D}_e = \begin{bmatrix} \lambda+2G & \lambda & \lambda & 0 & 0 & 0 & 0 \\ \lambda & \lambda+2G & \lambda & 0 & 0 & 0 & 0 \\ \lambda & \lambda & \lambda+2G & 0 & 0 & 0 & 0 \\ 0 & 0 & 0 & G+G_c & G-G_c & 0 & 0 \\ 0 & 0 & 0 & G-G_c & G+G_c & 0 & 0 \\ 0 & 0 & 0 & 0 & 0 & 2G & 0 \\ 0 & 0 & 0 & 0 & 0 & 0 & 2G \end{bmatrix} \tag{8}$$

with the Lame constant $\lambda = 2G\upsilon/(1-2\upsilon)$, G and υ are the shear modulus and Poisson's ratio in the classical sense, while G_c is introduced as the Cosserat shear modulus.

2.2 3D Cosserat continuum

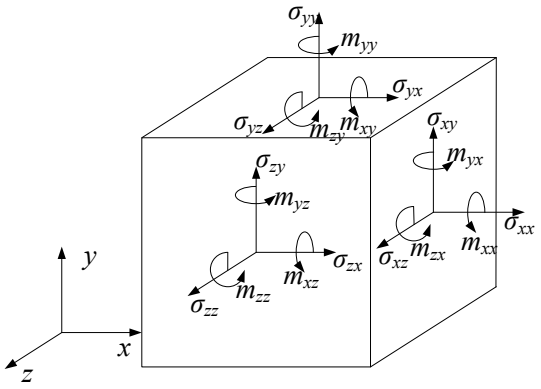

Fig. 2 Stress and couple stress in a 3D Cosserat continuum

In three dimensional Cosserat continuum, there are six independent degrees of freedom at each material point, i.e. three conventional translational degrees-of-freedom (u_x, u_y, u_z) and three rotational degrees of freedom $(\omega_x, \omega_y, \omega_z)$. The subscript of the translational degrees-of-freedom represents the direction of the displacement, and the subscript of the rotational degrees-of-freedom represents the axis around which the rotation revolves. The number of mechanical variables increases from 7 in two dimensions to 18 which includes nine conventional stresses and nine couple-stresses shown in Fig. 2. The stress vector and stress components are defined as

$$\begin{aligned} \boldsymbol{\sigma} = \{ & \sigma_{xx} \quad \sigma_{yy} \quad \sigma_{zz} \quad \sigma_{xy} \quad \sigma_{yx} \quad \sigma_{yz} \quad \sigma_{zy} \quad \sigma_{zx} \quad \sigma_{xz} \quad m_{xx}/l_t \quad m_{yy}/l_t \quad m_{zz}/l_t \\ & m_{xy}/l_b \quad m_{xz}/l_b \quad m_{yx}/l_b \quad m_{yz}/l_b \quad m_{zx}/l_b \quad m_{zy}/l_b \}^{\mathrm{T}} \end{aligned} \tag{9}$$

where m_{xx}, m_{yy}, m_{zz} are introduced as torsional couple stresses and $m_{xy}, m_{xz}, m_{yx}, m_{yz}, m_{zx}, m_{zy}$ are introduced as bending couple stresses in three dimensional Cosserat theory, l_{t} and l_{b} are defined as the internal length scales associated with

torsion and bending items respectively(Gauthier et al 1975; Eringen 1999). Correspondingly, there are 18 strain components in three dimensional Cosserat continuum. Each rotational degrees-of-freedom causes a torsional micro-curvature $\kappa_{ij} = \frac{\partial \omega_i}{\partial x_j}$ (i=j) at its spin axis and the other two bending micro-curvature $\kappa_{ij} = \frac{\partial \omega_i}{\partial x_j}$ (i≠j) at another two axes. The strain vector and strain components can be expressed as

$$\begin{aligned}\boldsymbol{\varepsilon} = \{ & \varepsilon_{xx} \quad \varepsilon_{yy} \quad \varepsilon_{zz} \quad \varepsilon_{xy} \quad \varepsilon_{yx} \quad \varepsilon_{yz} \quad \varepsilon_{zy} \quad \varepsilon_{zx} \quad \varepsilon_{zx} \quad \kappa_{xx} l_t \quad \kappa_{yy} l_t \quad \kappa_{zz} l_t \\ & \kappa_{xy} l_b \quad \kappa_{xz} l_b \quad \kappa_{yx} l_b \quad \kappa_{yz} l_b \quad \kappa_{zx} l_b \quad \kappa_{zy} l_b \}^{\mathrm{T}}\end{aligned} \tag{10}$$

in which $\kappa_{xx}, \kappa_{yy}, \kappa_{zz}$ are the torsional micro-curvatures, and $\kappa_{xy}, \kappa_{xz}, \kappa_{yx}, \kappa_{yz}, \kappa_{zx}, \kappa_{zy}$ are the bending micro-curvatures.

The relation between strain components and displacement components and the equilibrium equations can be written in matrix – vector forms as

$$\boldsymbol{\varepsilon} = \mathbf{L}\mathbf{u} \; ; \quad \mathbf{u} = \{ u_x \quad u_y \quad u_z \quad \omega_x \quad \omega_y \quad \omega_z \}^{\mathrm{T}} \tag{11}$$

$$\mathbf{L}^{\mathrm{T}}\boldsymbol{\sigma} + \mathbf{f} = \mathbf{0} \tag{12}$$

in which the operator matrix

$$\boldsymbol{L}^T = \begin{pmatrix} \frac{\partial}{\partial x} & 0 & 0 & 0 & \frac{\partial}{\partial y} & 0 & 0 & \frac{\partial}{\partial z} & 0 & 0 & 0 & 0 & 0 & 0 & 0 & 0 & 0 & 0 \\ 0 & \frac{\partial}{\partial y} & 0 & \frac{\partial}{\partial x} & 0 & 0 & \frac{\partial}{\partial z} & 0 & 0 & 0 & 0 & 0 & 0 & 0 & 0 & 0 & 0 & 0 \\ 0 & 0 & \frac{\partial}{\partial z} & 0 & 0 & \frac{\partial}{\partial y} & 0 & 0 & \frac{\partial}{\partial x} & 0 & 0 & 0 & 0 & 0 & 0 & 0 & 0 & 0 \\ 0 & 0 & 0 & 0 & 0 & -1 & 1 & 0 & 0 & l_t \frac{\partial}{\partial x} & 0 & 0 & l_b \frac{\partial}{\partial y} & l_b \frac{\partial}{\partial z} & 0 & 0 & 0 & 0 \\ 0 & 0 & 0 & 0 & 0 & 0 & 0 & -1 & 1 & 0 & l_t \frac{\partial}{\partial y} & 0 & 0 & 0 & l_b \frac{\partial}{\partial x} & l_b \frac{\partial}{\partial z} & 0 & 0 \\ 0 & 0 & 0 & -1 & 1 & 0 & 0 & 0 & 0 & 0 & 0 & l_t \frac{\partial}{\partial z} & 0 & 0 & 0 & 0 & l_b \frac{\partial}{\partial x} & l_b \frac{\partial}{\partial y} \end{pmatrix} \tag{13}$$

Similar with two dimensional problem, the elastic strain vector $\boldsymbol{\varepsilon}_e$ is linearly related to the stress vector,

$$\boldsymbol{\sigma} = \mathbf{D}_e \boldsymbol{\varepsilon}_e \tag{14}$$

in which the elastic modulus matrix $\mathbf{D}_e$ for isotropic media can be given in the form

$$\boldsymbol{D_e} = \begin{pmatrix} \boldsymbol{D_u} & \mathbf{0} \\ \mathbf{0} & \boldsymbol{D}_\omega \end{pmatrix} \tag{15}$$

$$\boldsymbol{D}_u = \begin{pmatrix} \lambda+2G & \lambda & \lambda & 0 & 0 & 0 & 0 & 0 & 0 \\ \lambda & \lambda+2G & \lambda & 0 & 0 & 0 & 0 & 0 & 0 \\ \lambda & \lambda & \lambda+2G & 0 & 0 & 0 & 0 & 0 & 0 \\ 0 & 0 & 0 & G+G_c & G-G_c & 0 & 0 & 0 & 0 \\ 0 & 0 & 0 & G-G_c & G+G_c & 0 & 0 & 0 & 0 \\ 0 & 0 & 0 & 0 & 0 & G+G_c & G-G_c & 0 & 0 \\ 0 & 0 & 0 & 0 & 0 & G-G_c & G+G_c & 0 & 0 \\ 0 & 0 & 0 & 0 & 0 & 0 & 0 & G+G_c & G-G_c \\ 0 & 0 & 0 & 0 & 0 & 0 & 0 & G-G_c & G+G_c \end{pmatrix} \tag{16}$$

$$\mathbf{D}_{\boldsymbol{\omega}} = \begin{bmatrix} 2G & 0 & 0 & 0 & 0 & 0 & 0 & 0 & 0 \\ 0 & 2G & 0 & 0 & 0 & 0 & 0 & 0 & 0 \\ 0 & 0 & 2G & 0 & 0 & 0 & 0 & 0 & 0 \\ 0 & 0 & 0 & 2G & 0 & 0 & 0 & 0 & 0 \\ 0 & 0 & 0 & 0 & 2G & 0 & 0 & 0 & 0 \\ 0 & 0 & 0 & 0 & 0 & 2G & 0 & 0 & 0 \\ 0 & 0 & 0 & 0 & 0 & 0 & 2G & 0 & 0 \\ 0 & 0 & 0 & 0 & 0 & 0 & 0 & 2G & 0 \\ 0 & 0 & 0 & 0 & 0 & 0 & 0 & 0 & 2G \end{bmatrix} \tag{17}$$

where λ, G, υ and G_c are the same as those in two dimensions.

3. Pressure dependent Cosserat elastoplastic model

The Drucker-Prager yield criterion is particularly considered to describe the pressure dependent elastoplastic constitutive behavior of the geotechnical medium, and is written in the following form

$$F = q + A_\phi \sigma_h + B = 0 \tag{18}$$

in which the effective deviatoric stress q and the hydrostatic stress σ_h characterizing the second and the first stress invariants respectively can be expressed by

$$q = \left(\frac{1}{2}\boldsymbol{\sigma}^{\mathrm{T}}\mathbf{P}\boldsymbol{\sigma}\right)^{\frac{1}{2}}; \qquad \sigma_h = \frac{1}{\sqrt{3}}\left(\sigma_{xx} + \sigma_{yy} + \sigma_{zz}\right) \tag{19}$$

The material parameters and the plastic potential matrix for the case of the isotropic plasticity in the plane strain problem can be given as

$$A_\phi = \frac{2Sin\phi}{\sqrt{3}(3 - Sin\phi)} \qquad B = \frac{-6cCos\phi}{\sqrt{3}(3 - Sin\phi)} \tag{20}$$

where

$$\mathbf{P}=\begin{bmatrix} 2 & -1 & -1 & 0 & 0 & 0 & 0 \\ -1 & 2 & -1 & 0 & 0 & 0 & 0 \\ -1 & -1 & 2 & 0 & 0 & 0 & 0 \\ 0 & 0 & 0 & 3/2 & 3/2 & 0 & 0 \\ 0 & 0 & 0 & 3/2 & 3/2 & 0 & 0 \\ 0 & 0 & 0 & 0 & 0 & 3 & 0 \\ 0 & 0 & 0 & 0 & 0 & 0 & 3 \end{bmatrix} \tag{21}$$

for two dimensional problems concerned; while

$$\mathbf{P}=\begin{pmatrix} \mathbf{P}_1 & \mathbf{0} & \mathbf{0} \\ \mathbf{0} & \mathbf{P}_2 & \mathbf{0} \\ \mathbf{0} & \mathbf{0} & \mathbf{P}_3 \end{pmatrix} \tag{22}$$

for three dimensional problems concerned, where $\mathbf{P}_1, \mathbf{P}_2$ and $\mathbf{P}_3$ can be expressed as

$$\mathbf{p}_1=\begin{pmatrix} 2 & -1 & -1 \\ -1 & 2 & -1 \\ -1 & -1 & 2 \end{pmatrix}, \mathbf{p}_2=\begin{pmatrix} \frac{3}{2} & \frac{3}{2} & 0 & 0 & 0 & 0 \\ \frac{3}{2} & \frac{3}{2} & 0 & 0 & 0 & 0 \\ 0 & 0 & \frac{3}{2} & \frac{3}{2} & 0 & 0 \\ 0 & 0 & \frac{3}{2} & \frac{3}{2} & 0 & 0 \\ 0 & 0 & 0 & 0 & \frac{3}{2} & \frac{3}{2} \\ 0 & 0 & 0 & 0 & \frac{3}{2} & \frac{3}{2} \end{pmatrix}, \mathbf{p}_3=\begin{pmatrix} 3 & 0 & 0 & 0 & 0 & 0 & 0 & 0 & 0 \\ 0 & 3 & 0 & 0 & 0 & 0 & 0 & 0 & 0 \\ 0 & 0 & 3 & 0 & 0 & 0 & 0 & 0 & 0 \\ 0 & 0 & 0 & 3 & 0 & 0 & 0 & 0 & 0 \\ 0 & 0 & 0 & 0 & 3 & 0 & 0 & 0 & 0 \\ 0 & 0 & 0 & 0 & 0 & 3 & 0 & 0 & 0 \\ 0 & 0 & 0 & 0 & 0 & 0 & 3 & 0 & 0 \\ 0 & 0 & 0 & 0 & 0 & 0 & 0 & 3 & 0 \\ 0 & 0 & 0 & 0 & 0 & 0 & 0 & 0 & 3 \end{pmatrix} \tag{23}$$

with the cohesion c and the internal frictional angle ϕ . With the piecewise linear hardening/softening assumption for the cohesion, we have

$$c=c\left(\bar{\varepsilon}_p\right)=c_0+h_p^c\bar{\varepsilon}_p \tag{24}$$

where c_0 is the initial cohesion, h_p^c the hardening/softening parameter for cohesion, $\bar{\varepsilon}_p$ the equivalent plastic strain. It has been found that using the classical definition of equivalent plastic strain can not accurately capture different post yield paths in tension and compression simultaneously. An equivalent plastic strain measure capable of capturing the behavior of a material, which is characterized by two different strain

hardening/softening curves produced by loading in tension and then compression, is defined as (Li et al 1994; Duxbury and Li 1996)

$$\Delta\bar{\varepsilon}_p = \Delta\lambda\left(1+\frac{\sigma_h}{|\sigma_h|}\frac{A_\psi}{\sqrt{3}}\right) \tag{25}$$

where $\Delta\lambda$ is the plastic multiplier defined in non-associated flow rule

$$\Delta\boldsymbol{\varepsilon}_p = \Delta\lambda\frac{\partial G}{\partial\boldsymbol{\sigma}} \tag{26}$$

The plastic potential function is taken in the form

$$G = q + A_\psi\sigma_h + B \tag{27}$$

with the material parameter

$$A_\psi = \frac{2Sin\,\psi}{\sqrt{3}(3-Sin\,\psi)} \tag{28}$$

ψ is the plastic potential angle (the angle of dilatance) defined by the deviatoric associativity rule. The material will be of associated plasticity as $\psi = \phi$.

In the framework of Cosserat continuum theory, a consistent algorithm of the pressure-dependent elastoplastic model, i.e. the return mapping algorithm for the integration of the rate constitutive equation and the closed form of the consistent elastoplastic tangent modulus matrix, has been derived for two dimensional problems (Li and Tang 2005). For three dimensional problem, we also develop a similar pressure-dependent elastoplastic model based on the detailed study of the characteristics of the three dimensional Cosserat continuum. The capability and performance of the present models for two and three dimensional Cosserat continuum in simulating strain localization problems are testified in the following parts.

4. The Finite Elements for Cosserat Continuum in two and three dimensions

The finite element used in the present simulation, should possess, in addition to the usual requirements to element intrinsic properties, the capability to capture the pronounced localized failure mode and to simulate the reduction of the load-carrying capability due to strain softening. As the properties of volumetric locking for low-order elements still exist in Cosserat continuum despite the introduction of microrotation ω, the high-order elements with reduced integration, which possess better performance in this issue, are used in the present work.

In this work, the eight nodded displacement-based quadrilateral isoparametric element interpolation approximation, as illustrated in Fig. 3(a), is simply employed for

the three degrees-of-freedom u_x, u_y, ω_z in the 2D Cosserat continuum, and the twenty nodded displacement-based solid isoparametric element interpolation approximation, as can be seen in Fig. 3(b), is simply employed for the six degrees-of-freedom, including three-translational (u_x, u_y, u_z), and three-rotational degrees-of-freedom $(\omega_x, \omega_y, \omega_z)$ in the 3D Cosserat continuum.

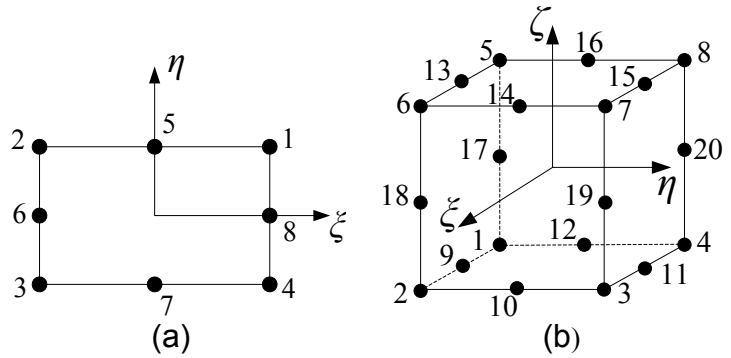

Fig. 3 The finite elements used for Cosserat continuum: (a) eight nodded finite element for 2D problem; (b) twenty nodded solid finite element for 3D problem

5. Numerical examples

5.1 Analysis for the size effect of micro-structure

Some experiments of micro-structures show that the mechanical strengths of the micro-structures depend on their size largely, i.e. size effects (Fleck et al 1994; Stolken and Evans 1998). To reflect the size effects of micro-structures, one of the effective methods is to use Cosserat continuum theory, in which the material parameters defined as internal length scale are included to describe the mechanical behavior of such micro-structures. Consider a micro-cantilever beam subjected to a 10MPa transverse shear traction at the free end of the beam. The geometry and boundary conditions of the beam, and relevant 20-nodes FE grid partition form are shown in Fig. 4, where l/h=8 and b/h=2. The Young's modulus and the Poisson's ratio of the material are 20 GPa and 0.3 respectively. The Cosserat shear modulus is 5 GPa and $l_b = l_t = l_c = 250\mu\text{m}$.

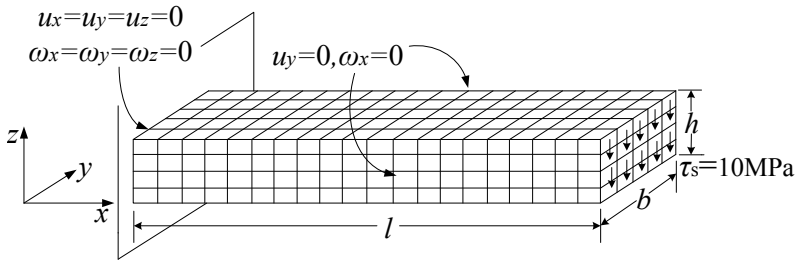

Fig. 4 Geometry and boundary conditions for the micro-cantilever beam

According to Timoshenko and Goodier (1970), the analytical solution for the deflection of the free end of the cantilever beam is

$$u_y = \frac{4\tau_s l^3}{Eh^2}\left(1-\upsilon^2\right) \tag{29}$$

For several different sizes of the beam, i.e. several different value of h/l_c, the analytical solution and the numerical solutions based on classical continuum theory (FEM) and Cosserat continuum theory (Cosserat-FEM) for the deflection of the free end of the cantilever beam are obtained. Table 1 gives the results as h/l_c=1, 2, 4, 6, 10, 20 respectively.

It can be seen that the FEM solutions are much closed to analytical solutions since both of them are based on classical continuum theory, but based on Cosserat continuum theory, the Cosserat-FEM solutions are quite different. As the size of the micro-cantilever beam is closed to the internal scale l_c, the Cosserat-FEM solutions are getting much smaller than the analytical solutions and FEM solutions; as the size of the micro-cantilever beam far outweighs the internal scale l_c, the Cosserat-FEM solutions are getting closed to analytical solutions and FEM solutions. It reveals that the numerical solutions based on Coseerat continuum theory are effective in modeling size effect of micro-structures.

Table 1 The values of deflection of the micro-cantilever beam in different cases

h/l_c	Analytical solution (μm)	FEM(μm)	Cosserat FEM(μm)
1	232.96	234.86	26.36
2	465.92	469.72	153.24
4	931.84	939.43	616.63
6	1397.76	1409.14	1141.87
10	2329.6	2348.57	2164.24
20	4659.2	4697.14	4596.53

5.2 Investigation of mesh-independent solutions

As strain softening constitutive behavior is incorporated into a computational model in the frame of classical plastic continuum theories, the initial and boundary value problem of the model will become ill-posed, resulting in pathologically mesh-dependent solutions. To illustrate the capability of the Cosserat continuum finite element in overcoming mesh-dependent solutions, a shear structure in two and three dimensional space is considered respectively.

5.2.1 Analysis of Two dimensional shear structure

The shear structure with a height of 0.2m in y' axis and an infinite length in the z' axis is considered as a two dimensional plane strain problem. Two regular uniform meshes with different mesh densities, i.e. 20×1, 40×1 element discretizations, are utilized as illustrated in Figures 5(a) and (b). All nodal displacements in the y' axis are prevented. The bottom of the shear structure is fixed and a monotonously increasing displacement in the x' axis enforced at the nodes on the upper boundary is prescribed. The material parameters used in this example are chosen as: E=1.0E+10Pa, υ=0.25, G_c=2.0E+9Pa, c_0=1.0E+8Pa, h_p^c=-5.0E+8Pa, l_c=0.006m. The rotational degrees of freedom at the nodes on the top and the bottom boundaries

are fixed to trigger the shear band in the shear structure.

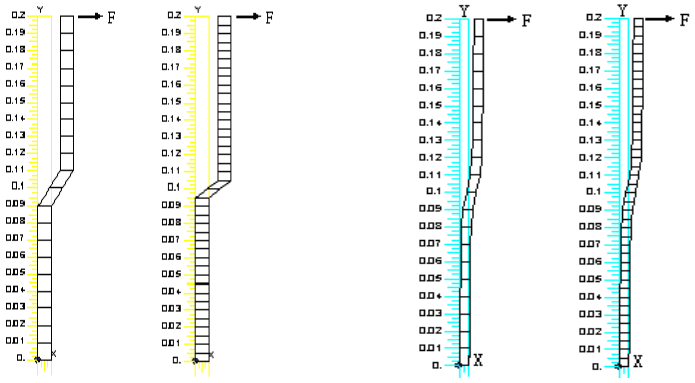

Fig. 5 Deformed configuration of the shear structure subjected to a prescribed transverse displacement u=7.5mm in the x-axis at the top of the structure: (a) classical continuum; (b) Cosserat continuum

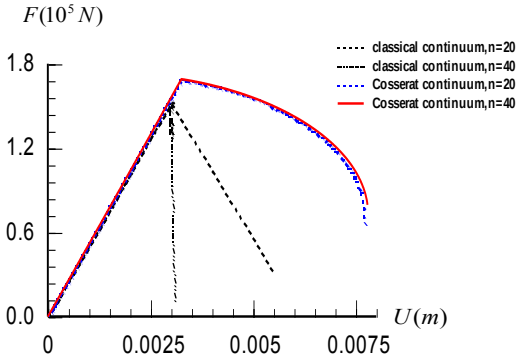

Fig. 6 Curves of the transverse load applied to the top of the structure with increasing prescribed transverse displacement U of the top surface with different mesh densities.

Figures 5 and 6 illustrate the deformed configurations and gradual reduction of the load-carrying capability for different mesh densities of shear structure due to strain softening with the development of plastic strains, where the shear structure is treated as the classical continuum and Cosserat continuum respectively. They illustrate that the load-displacement curves of the structure with different mesh densities converge to a physically realistic solution independent on the mesh density for Cosserat continuum, while pathologically mesh-dependent solutions for classical one.

5.2.2 Analysis of three dimensional shear structure

Consider the shear structure above with a finite length of 0.005m in the z axis as a three dimensional space problem. The geometry and boundary conditions and the material parameters used in this example are almost the same as those above. The internal length scales is chosen as $l_b = l_t = l_c = 250\mu\text{m}$. Figures 7 and 8 illustrate the deformed configurations and the load-carrying capability for different mesh densities as

the shear structure is treated as the classical continuum and Cosserat continuum respectively. The similar results can be seen in this example, i.e. a physically realistic solution independent on the mesh density for Cosserat continuum, while pathologically mesh-dependent solutions for classical one.

Fig. 7 Deformed configuration of the shear structure subjected to a prescribed transverse displacement u=7.5mm in the x-axis at the top of the structure: (a) classical continuum; (b) Cosserat continuum

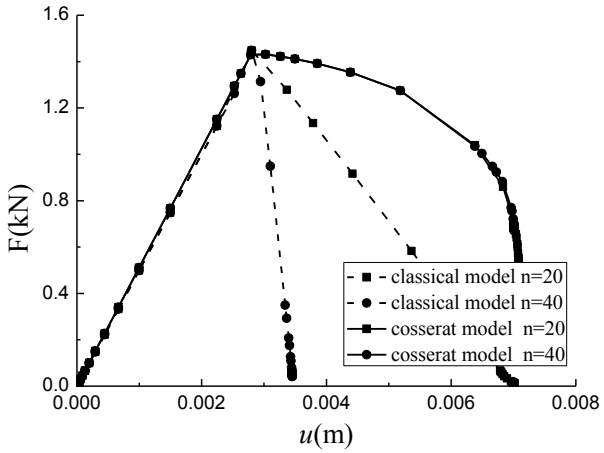

Fig. 8 Curves of the transverse load applied to the top of the structure with increasing prescribed transverse displacement U of the top surface with different mesh densities.

5.3 Investigate the well-posedness of the boundary value problem with strain softening behavior

5.3.1 Investigate the stability of a vertical cut in two dimensions

Investigate the stability of a vertical cut in two dimensional soil with strain softening material. In this investigation, a finite element mesh is created in a 13.2×6.8m rectangular block of soil. The material parameters of the soil are chosen as E =5.0E+4kPa, ν =0.3, G_c =1.0E+4kPa, c_0 =30kPa, h_p^c =-30kPa, ρ =2.0E3kg/m3. Before the excavation, the initial stress state within the soil has been reproduced by progressively increasing the gravity acceleration up to the value of 9.81 $\mathrm{m/s^2}$, assuming

that the soil exhibit elastic perfectly plastic behavior with the Drucker-Prager yielding criterion. At the end of gravity loading, the displacements and strains are reset to zero. The excavation process is simulated by removing 8 elements at the same level in one increment from the upper left corner of the initial finite element mesh. Mana's method is used to calculate the excavation loading (Mana and Clough 1981).

At first, the computational model in the frame of classical continuum theory is used to analyze the excavation process. Fig. 9(a) shows the effective plastic strain distribution after the removal of 10th layer, and it can be seen that the failure zone does not run through and the whole failure has not been achieved. As the excavation process continues, the classical finite element numerical solution faces significant difficulties that the numerical calculation can not be carried out any more due to the increasing number of negative eigenvalues in the system stiffness matrix.

Then, the computational model in the frame of Cosserat continuum theory is used to analyze the excavation process. Fig. 9(b) shows the effective plastic strain distribution after the removal of 10th layer, which is almost the same as Fig. 9(a). As the excavation process continues and the elements of 11th layer are removed, the numerical calculation continues also. Fig. 9(c) shows that the maximum value and the distribution area of the effective plastic strain increase largely after the removal of 11th layer. It can be seen that a whole trans-failure zone has formed. Therefore, the numerical results in the present study indicate the inability of classical continuum model in simulating the whole failure progress, while the capability and performance of Cosserat continuum model in keeping the well-posedness of the boundary value problems with strain softening behavior incorporated and in completing simulation of the whole failure progress.

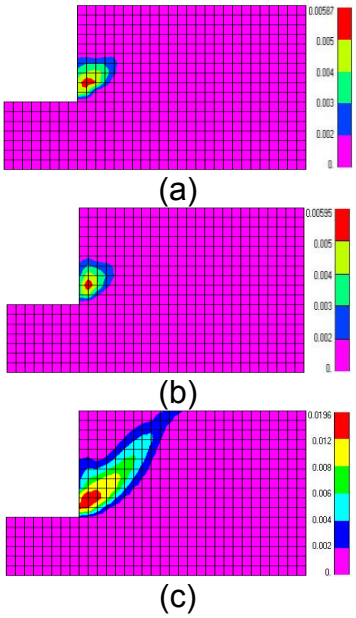

Fig. 9 Effective plastic strain distribution in the vertical cut: (a) after the removal of 10th layer with classical continuum; (b) after the removal of 10th layer with Cosserat continuum; (c) after the removal of 11th layer with Cosserat continuum.

5.3.2 Investigate the stability of a vertical cut in three dimensions

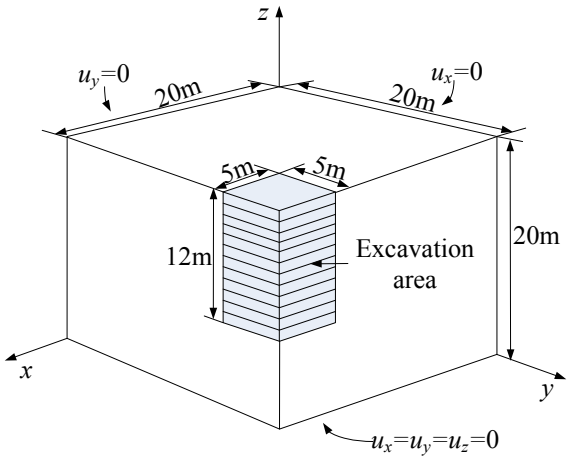

Fig. 10 The geometry and boundary conditions of the model.

Investigate the stability of a vertical cut in three dimensional soil with strain softening material. The dimensions of the soil space are considered as 40m×40m×40m, in which the cut area in horizontal plane is 10m×10m. Owing to symmetry condition, the calculation is carried out only for a quarter of the soil space, which is discretized by regular $n\times n\times n$ meshes. The displacements in x', y' and z' axes of the nodes on the bottom boundary are specified as null. The finite element nodes on the left side boundary are fixed in y' axis and free in x' and z' axes respectively, while the finite element nodes on the back side boundary are fixed in x' axis and free in y' and z' axes respectively. The material parameters of the soil are chosen as: $l_b = l_t = l_c = 0.05\mathrm{m}$, the other parameters are the same as that of two dimensions. The analysis process is also analogous to that in two dimensions. The excavation process is simulated by removing 5×5 elements at the same level in one increment from the upper center of the initial finite element mesh.

At first, the classical plastic continuum theory is used to analysis the excavation process. Fig. 11(a) shows the effective plastic strain distribution after the removal of 7th layer, and it can be seen that the failure zone does not run through and the whole failure has not been achieved. As the excavation process continues, the classical finite element numerical solution faces significant difficulties that the numerical calculation can not be carried out any more due to the increasing number of negative eigenvalues in the system stiffness matrix.

Then, Cosserat plastic continuum theory is used to analysis the excavation process. Fig. 11(b) shows the effective plastic strain distribution after the removal of 7th layer, which is extended up to the surface of the soil. As the excavation process continues and the elements of 8th layer are removed, the numerical calculation continues also. Fig. 11(c) shows that the maximum value and the distribution area of the effective plastic strain increase largely after the removal of 8th layer. It can be seen that a whole trans-failure zone has been completed. Therefore, the numerical results in the three dimensional study indicate the inability of classical continuum model in simulating the whole failure progress, while the capability and performance of Cosserat continuum

model in keeping the well-posedness of the boundary value problems with strain softening behavior incorporated and in completing simulation of the whole failure progress. It should be pointed out that the excavation depth in three dimensional soil is greater than that in two dimensional soil due to the three dimensional space effects. Fig. 12 displays the distributions of the micro-rotation in this condition, which illustrates obvious rotation in the failure area, so the micro-rotation is also an important indication that phenomena of strain localization occur.

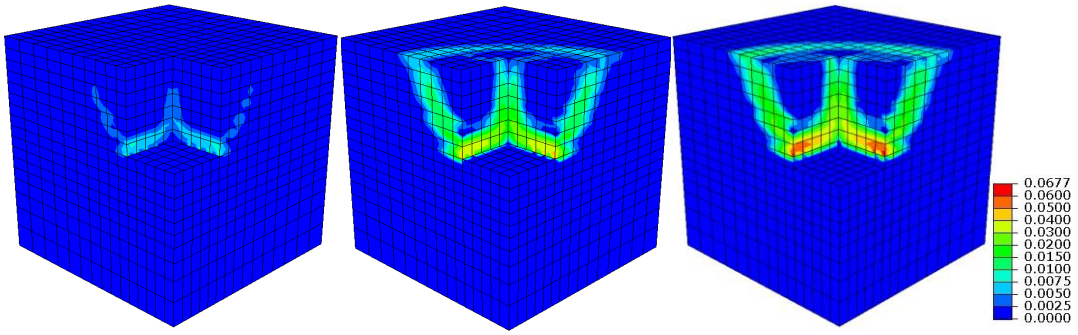

(a) (b) (c)

Fig. 11 Effective plastic strain distribution in the vertical excavation: (a) after the removal of 7th layer with classical continuum; (b) after the removal of 7th layer with Cosserat continuum; (c) after the removal of 8th layer with Cosserat continuum.

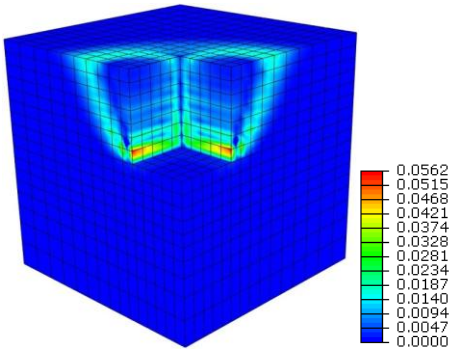

Fig. 12 Rotational quantity distributions in the vertical cut after the removal of 8th layer with Cosserat continuum

5.4 Investigate the well-posedness of the boundary value problem with non-associated elastoplastic behavior

As non-associated plastic behavior incorporated, the material may exhibit an equivalent strain softening behavior in some circumstances (Pande et al. 1986). A gravity retaining wall in passive condition is considered. As show in Fig. 13, the height of the wall is $H(=3.2\mathrm{m})$ and the soil behind the wall has a unit density of ρ=2.0E3kg/m3. The material parameters of the soil are chosen as: E =5.0E+4kPa, ν =0.35, G_c=1.0E+4kPa, $l_c=0.12\mathrm{m}$. The other material parameters of the soil are chosen for three different cases as:① c_0=50kPa, $\varphi=35^\circ$, $\psi=0^\circ$; ② c_0=50kPa, $\varphi=40^\circ$, $\psi=0^\circ$;

③ c_0 =40kPa, $\varphi = 35^\circ$, $\psi = 0^\circ$. It is assumed that the friction between the wall and soil is zero. A 13.2×6.8m rectangular block of soil is selected to create the finite element mesh, in which the right border and left border under the wall and bottom are fixed. Fig. 14 gives the curves of force (acting on the wall) -displacement (of the wall) for these cases when classical continuum theory and Cosserat continuum theory are considered separately.

For case 1, the results based on classical continuum theory shows that the force-displacement curve stops at a relatively early stage due to the difference between friction angle and dilation angle. But for Cossserat continuum theory, the force-displacement curve exhibits an equivalent strain softening behavior and that the displacement can extend to 0.2m. The limit loads for these two theories are almost the same.

For case 2, a larger difference between friction angle and dilation angle is adopted to increase difficulties in numerical calculation. In this case, more serious difficulties are encountered for classical continuum theory and the finite element numerical calculation can not be carried out, so there are no records in Fig. 14. But it is not the case for Cosserat continuum theory, according to which the numerical difficulties are overcome and the force-displacement curve and an equivalent strain softening behavior are obtained.

For case 3, the difference between friction angle and dilation angle is the same as case 1, but the cohesion is decreased from 50kPa to 40kPa. In this case, the results analogous with that of case 2 are obtained.

Fig. 15 give deformation configuration and effective plastic strain distribution for classical continuum($\varphi = 35^\circ, \psi = 0^\circ$), which show the local sharply outstanding deformation and the intense narrow band distribution of effective plastic strain due to local constitutive model used. Fig. 16 give deformation configuration and effective plastic strain distribution for Cosserat continuum($\varphi = 35^\circ, \psi = 0^\circ$), which show the local relaxing deformation and certain wide band distribution of effective plastic strain due to non-local constitutive model with an internal length scale used.

Numerical results indicate the inability of classical continuum model, while the capability and performance of Cosserat continuum model in keeping the well-posedness of the boundary value problems with non-associated perfect elastoplastic behavior incorporated.

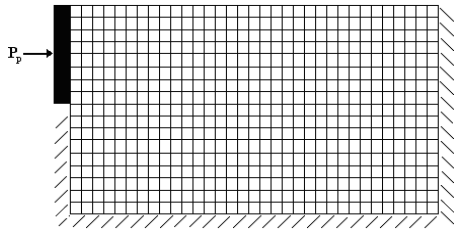

Fig. 13 Passive earth pressure on retaining wall: boundary conditions and finite element mesh.

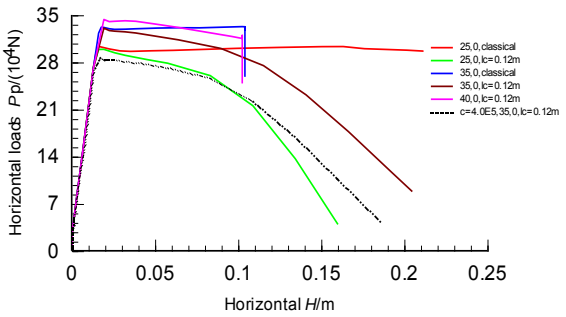

Fig. 14 Force-displacement curves of retaining wall for different cases.

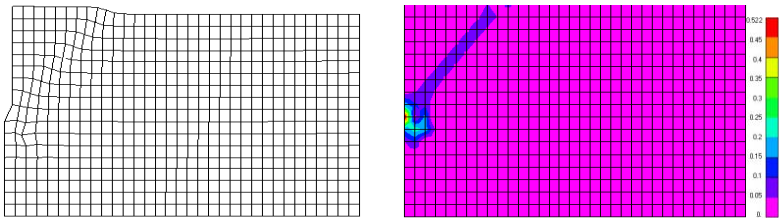

Fig. 15 Classical continuum ($\varphi = 35^\circ$, $\psi = 0^\circ$): (a)deformation configuration; (b) Effective plastic strain distribution.

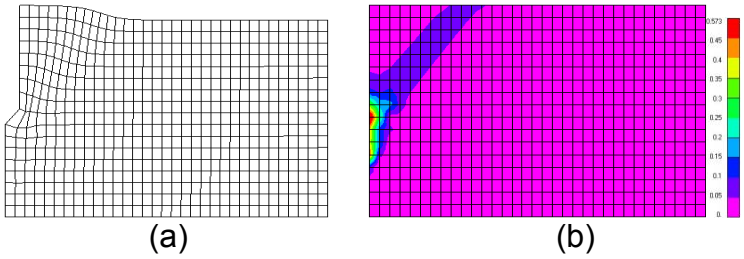

Fig. 16 Cosserat continuum($\varphi = 35^\circ$, $\psi = 0^\circ$): (a) deformation configuration; (b) effective plastic strain distribution.

6. Conclusions

Based on the analysis for the characteristics of 2D and 3D Cosserat continuum, this paper presents the elastoplastic Cosserat continuum models and corresponding finite element numerical methods for both 2D and 3D pressure-dependent materials. With these models and finite element methods, the size effects of a cantilever beam, the mesh-independent solution of a shear structure, the strain localization failure due to strain softening in excavation and the strain localization failure due to material dilatancy in retaining structure are studied. Numerical results illustrate that as compared with the performance of the finite element procedure based on the classical continuum model, the present finite element methods based on the proposed Cosserat continuum model are capable of reflecting the size effects, ensuring mesh- independent solution,

preserving the well-posedness of the boundary value problem characterized by the strain localization due to strain softening and material dilatancy and simulating the entire progressive failure process occurring in engineering structures.

Acknowledgements

The authors are pleased to acknowledge the support of this work by the National Natural Science Foundation of China through contract/grant numbers 50808033, the National Key Basic Research and Development Program (973 Program) through contract number 2010CB731502 and the Fundamental Research Funds for the Central Universities (DUT11LK37, DUT11ZD110).

References

Troncone, A. (2005), "Numerical analysis of a landslide in soils with strain-softening behaviour," *Geotechnique*, **55**(8), 585-596.

Pande, G.N., Pietruszczak, S. (1986), "Symmetric tangent stiffness formulation for non-associated plasticity," *Computers and Geotechnics*, **2**(2), 89-99.

Li, X.K., Zhang, J.B. and Zhang, H.W. (2002), "Instability of wave propagation in saturated poroelastoplastic media," *Int. J. Numer. Anal. Meth. Geomech*.,, **26**(6), 563-578.

Muhlhaus, H.B. and Vardoulakis, I. (1987), "The thickness of shear bands in granular materials," *Geotechnique*, **37**(3), 271-283.

Muhlhaus, H.B. (1989). "Application of Cosserat theory in numerical solutions of limit load problems," *Ing. Arch*., **59**(2), 124-137.

de Borst, R. and Sluys L.J. (1991), "Localization in a Cosserat continuum under static and dynamic loading conditions," *Comput. Methods Appl. Mech. Engrg.*, **90**(1), 805-827.

de Borst, R. (1991), "Simulation of strain localization: a reappraisal of the Cosserat continuum," *Eng. Comput.*, **8**(4), 317-332.

de Borst, R. (1993), "A generalization of J2-flow theory for polar continua," *Comp. Meth. Appl. Mech. Eng.*, **103**(3), 347-362.

Tejchman, J. and Wu, W. (1993), "Numerical study on patterning of shear bands in a Cosserat continuum," *Acta Mech.*, **99**(1-4), 61-74.

Tejchman, J. and Bauer, E. (1996), "Numerical simulation of shear band formation with a polar hypoplastic constitutive model," *Computers and Geotechnics,* **19**(3), 221-244.

Steinmann, P. (1994), "A micropolar theory of finite deformation and finite rotation multiplicative elastoplasticity," *Int. J. Solids Struct.*, **31**(8), 1063-1084.

Steinmann, P. (1999), "Formulation and computation of geometrically nonlinear gradient damage," *Int. J. Numer. Meth. Eng.*, **46**(5), 757-779.

Iordache, M.M. and Willam, K. (1998), "Localized failure analysis in elastoplastic Cosserat continua," *Comput. Methods Appl. Mech. Eng.,* **151**(3), 559–586.

Manzari MT.(2004), "Application of micropolar plasticity to post failure analysis in geomechanics," *Int. J. Numer. Anal. Meth. Geomech*., **28**(10), 1011-1032.

Li, X.K. and Tang, H.X. (2005), “A consistent return mapping algorithm for pressure-dependent elastoplastic Cosserat continua and modeling of strain localization,” *Comput. Struct.*, **83**(1): 1-10.
Khoei, A.R., Gharehbaghi, S.A. and Tabarraie, A.R. (2007), “Error estimation, adaptivity and data transfer in enriched plasticity continua to analysis of shear band localization,” *Appl. Math. Model*, **31**(6), 983-1000.
Ehlers, W. and Volk, W. (1998), “On theoretical and numerical methods in the theory of porous media based on polar and non-polar elasto-plastic solid materials,” *Int. J. Solids Struct.,* **35**(34), 4597–4617.
Rubin, M.B. (2005), “Numerical solution of axisymmetric nonlinear elastic problems including shells using the theory of a Cosserat point,” *Comp. Mech.,* **36**(4), 266–288.
Liu, D., Cao, D.Q., Rosing, R. et al. (2007), “Finite element formulation of slender structures with shear deformation based on the Cosserat theory,” *Int. J. Solids Struct.,* **44**(24), 7785–7802.
Riahi, A. and Curran, J.H. (2009), “Full 3D finite element Cosserat formulation with application in layered structures,” *Appl. Math. Model,* **33**(8), 3450-3464.
Riahi, A., Curran, J.H. and Bidhendi, H. (2009) “Buckling analysis of 3D layered structures using a Cosserat continuum approach,” *Comput. Geotech.,* **36**(7), 1101-1112.
Khoei, A.R., Yadegari, S. and Biabanaki, S.O.R. (2010), “3D finite element modeling of shear band localization via the micro-polar Cosserat continuum theory,” *Comput Mater. Sci.,* **49**(4), 720-733.
Gauthier, R.D. and Jahsman, W.E. (1975), “A quest for micropolar elastic constants,” *J. Appl. Mech.,* **42**(2), 369-374.
Eringen, A.C. (1999), *Microcontinuum field theories, I: Foundations and Solids* ,Springer, New York.
Li, X.K., Duxbury, P.G. and Lyons, P. (1994), “Considerations for the application and numerical implementation of strain hardening with the Hoffman yield criterion,” *Comput. Struct.,* **52**(4), 633–644.
Duxbury, P.G. and Li, X.K. (1996), “Development of elasto-plastic material models in a natural co-ordinate system,” *Compt. Methods Appl. Mech. Eng.,* **135**(4), 283–306.
Fleck NA, Muller GM, Ashby MF, etc.. (1994), “Strain gradient plasticity: theory and experiment,” *Acta Metall. Mater.,* **42**(2), 475-487.
Stolken J.S. and Evans A.G. (1998), “A micro-bend test method for measuring the plasticity length scale,” *Acta Mater.*, **46**(14), 5109-5115.
Timoshenko, S.P. and Goodier, J.N. (1970) *Theory of elasticity*, (third edtion), McGraw-Hill, New York.
Mana, A.I. and Clough, G.W. (1981), “Prediction of movements for braced cuts in clay”, *Journal of Geotechnical Engineering Division*, **107**(6), 759-778.